# Analysis of Machining Parameters in Drilling of Biocompatible Composite: HAp-HDPE and HAp-UHMWPE

**Arpan Mondal, Suman Chatterjee, Anshuman Kumar Sahu,
Siba Sankar Mahapatra, and Chander Prakash**

## 1 Introduction

Composite materials are basically materials made from more than two constituent materials having diverse physical or chemical properties. When the materials are combined, it produces a material with different properties from the individual constituent materials. Each individual component remains separate and different within the finished composite material. Generally, composite materials consisting building materials of cements, concrete, reinforced plastics like fiber-reinforced polymer, metal composites, and ceramic composites. A bio-composite is a material made by a matrix (resin) and a reinforcement of natural fibers (usually derived from plants or cellulose). Orthopedic problems like wear in the joints, joint fracture, and bone defects are common these days due to heavy work load. Therefore, an alternative for grafting or implantation by orthopedic surgery is essentially required. Bone is said to be an ecclesiastical shape formed by constituents like calcium, carbonated hydroxyapatite, type I collagen, non-collagenous proteins, and water [1]. Mineral contents in bone tissue lie in the range of 50–70% [2, 3]. Flexibility, rigidity, and nutrient contents of bones depend upon collagen, minerals, and water present in the bone, respectively. Hydroxyapatite (HAp) [$Ca_{10}(PO_4)_6(OH)_2$] helps in constructing

A. Mondal
Department of Mechanical Engineering, National Institute of Technical Teachers Training and Research, Kolkata, India

S. Chatterjee · A. K. Sahu (✉) · S. S. Mahapatra
Department of Mechanical Engineering, National Institute of Technology Rourkela, Rourkela, Odisha, India

C. Prakash
Department of Industrial Engineering, Lovely Professional University, Phagwara, Punjab, India

the bone tissue [4]. HAp reinforced with polymers provides an option to generate synthetic bone with tailored mechanical, biological, and surgical functions [5]. Composites with reinforcement of Hap in polymers used in the recent period are HAp/ZrO$_2$, HAp/methacrylate, HAp/TCP (tricalcium phosphate), HAp/HDPE (high-density polyethylene), ultra-high molecular weight polyethylene (UHMWPE) composites, etc. to develop materials as bone substitute materials [6–10].

In many ways, these bones are grafted, Masatakadeie et al. [11] suggested artificial bone grafting and core decompression for continuous osteonecrosis of the femoral condyle in the knee. Interconnected ceramic hydroxyapatite in surgical treatment of bone gives an option for curettage of benign bone which gives an option in surgical uses [12–15]. Grafting of bones is done on the part of damage portion of the bone. Surgeons usually do grafting by drilling. The implant bones are needed to be secured by screw and nut. When drilling is carried out, important parameters of drilling need to be controlled, so that minimum taper and maximum circularity at entry and exit can be achieved. Machining parameters affecting drilling of bio-composites are HAp volume percentage, speed, feed, and drill diameter. Experiments are carried out as per Taguchi's L$_{16}$ orthogonal array with mixed-level design, varying the factors at different levels on a CNC MAXMILL machine (MTAB, India). Taguchi's design of experiment approach is used to obtain maximum information about the process with less number of experiments [16–18]. Tsao and Hocheng [19] have used Taguchi method for parametric analysis of thrust of force of drill. Erol [20] suggests that Taguchi method is a powerful tool for the optimization of cutting parameters. However, Taguchi method is suitable for the optimization of a single response. When multiple responses are dealt simultaneously, the method breaks down. Therefore, many methods have been suggested to deal with multiple responses. For example, Huang and Lin [21] suggested a regression and principal component analysis (PCA)-based method to obtain optimum injection molding parameters in a multiple quality characteristics situation. Tong et al. [22] have suggested that optimization of multi-responses by principal component analysis leads to superior result as the method takes into account correlation of responses. The responses for this work are circularity at entry, circularity at exit, and taper of the holes, and they are suspected to be correlated. Principal component analysis, a data reduction technique, is capable of expressing the correlated responses into uncorrelated principal components [22–27]. The percentage of variation explained by each component is considered as the weight for the component. A linear combination of weights and components is capable of expressing multiple responses in a single equivalent response.

## 2 Experimental Analysis

### 2.1 Preparation of Composites and Characterization

Hydroxyapatite (HAp) [Ca$_{10}$(PO$_4$)$_6$(OH)$_2$] powder is prepared by wet chemical precipitation route method by mixing calcium hydroxide (Ca(OH)$_2$) powder, orthophosphoric (H$_3$PO$_4$) acid, and ammonia (NH$_3$) solution [4, 28–32]. HAp is reinforced

with polymer to produce the composite materials which can possibly be implanted as artificial bone. In preparing HAp, first 10 g of calcium hydroxide is weighted in a weighing machine (Mettler Toledo India, 0.01 g accuracy). Water of weight nearly 40 times the weight of HAp is mixed to form the solution. The solution is mixed by a magnetic stirrer (Remi Equipments Pvt. Ltd., India) at 50 °C to 60 °C for 3–4 h. Then, ortho-phosphoric acid is mixed with the solution with a rate of 30 drops per minute by a burette and constantly stirred without heat input to the solution until the pH value reach to 8–10. When the pH value of the solution reduces below the threshold values, then ammonia solution is added to increase the pH value. After 5–6 h, the magnetic stirrer is stopped, and the mixer is kept for 12 h at room temperature. Then, precipitations of mixture are collected using a filter paper. HAp precipitations are dried at 80 °C in an oven and calcinated at 850 °C for 2–3 h in a muffle furnace and finally, powder HAp is obtained.

Sintered HAp powder and commercial grades of high-density polyethylene (HDPE) and ultra-high molecular weight polyethylene (UHMWPE) are mixed to fabricate composites (HAp-HDPE and HAp-UHMWPE) by micro-injection molding. Composites with different amounts of HAp (10, 20, 30, 40 vol%) are produced by mixing, melting, granulating, and injection molding. First, spray-dried HAp powder (density 3.154 g/cm$^3$ estimated by water immersion method and mean particle size of 19.94 μm) is mixed with polymer matrix with a DSM XPLORE microcompounder. The mixtures are then melted, granulated, and dried at 160 °C for 2 h prior to the next processing stage [33]. Then test specimens are produced by injection molding [34]. The micro-injection molding barrel temperature at different zones are 180 °C, 190 °C, 200 °C, 220 °C for zone 1, zone 2, zone 3, zone 4, respectively, for HAp-HDPE composite. The mold temperature is 60 °C and injection pressure of 14 MPa. The time spent for loading, holding, and cooling of HDPE is 4 s, 30 s, and 30 s, respectively.

Melt flow index of UHMWPE is very low (0.09 gm/10 min at 190 °C); hence, micro-injection molding is difficult due to fail of screw with high load. Therefore, compression molding route has been adopted. Sintered HAp powder and commercial grade UHMWPE is mixed in a Thermo Scientific (TSE 24 MC) twin screw extruder at a temperature between 180 °C and 220 °C. The extruded material is pelletized into granules and then twin screw extruded at 30 rpm. After granulation, compression molding technique is applied to get the composite sheets. The specimens are hot drawn at 100 °C having a cross-head speed of 50 mm/min. The granules are vacuum dried at 80 °C overnight to remove any traces solvent. A NEOPLAST hydraulic press (Model no-HP 80T) is used at operating temperature of 220 °C in both the top and the bottom plates and applying a pressure of 308 MPa. A contour cutter is used to cut the samples into required shape.

The XRD graph of HAp-HDPE composite is shown in Fig. 1 for different volume percentage of HAp. The high peaks show dry HAp in its pure form with reference code 74-0566.

Micro-structural examination is done by using JSM JEOL 6480 LV Scanning Electron Microscope (SEM) for both the composites. Micrographs indicate that
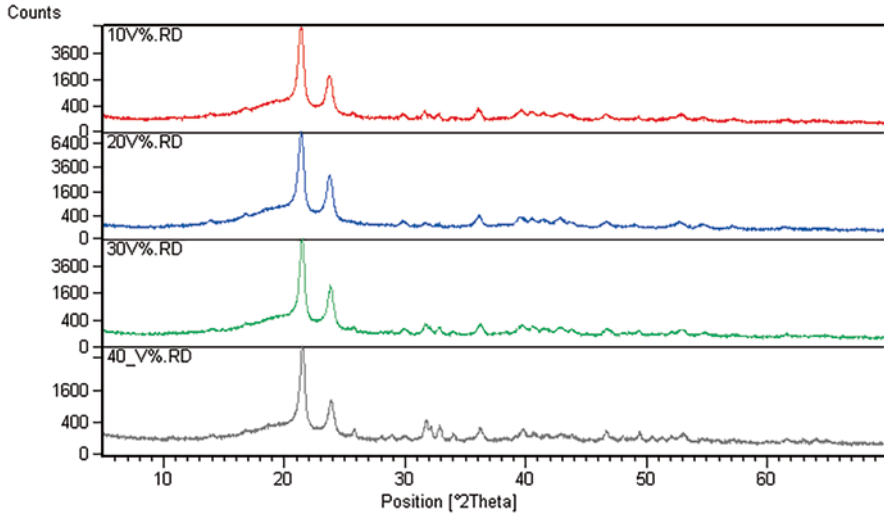
**Fig. 1** XRD graph for different vol. % of HAp with HDPE

HAp is uniformly distributed over the matrix. However, some globules are observed due to in homogenous mixing (Figs. 2 and 3).

The composites were prepared in standard laboratory atmosphere and ASTM standards are followed for preparing the specimens to perform different mechanical tests. Tensile, compressive, and flexural tests are carried out in INSTRON 3382 UTM machine. Impact test is carried out in Tinius Olsen Impact Systems IT406. The specifications for all tests are listed in Table 1.

The graph between Young's modulus versus HAp vol. % is shown in Fig. 4. It can be observed that both the composites exhibit maximum Young's modulus for 40 vol. % of HAp. However, HAp-UHMWPE composite shows higher Young's modulus for any volume percentage as compared to HAp-HDPE composite.

Figures 5, 6, and 7 show the graph between HAp vol. % with tensile strength, HAp vol. % versus compressive strength, HAp vol. % versus flexural strength, and HAp vol. % versus inter-laminar shear stress (ILSS), respectively. Figure 5 shows that tensile strength is decreasing with the increasing amount of HAp vol. % for both HAp-HDPE and HAp-UHMWPE composites. However, reduction of tensile strength with increase of HAp volume percentage is more pronounced for HAp-UHMWPE composite. Figure 6 shows that when the HAp vol. % is increased, compressive strength is decreased for HAp-UHMWPE composite. However, decrease of compressive strength with the increase of HAp vol. % is not appreciable in case of HAp-HDPE composite.

Flexural test is done by an INSTRON 3382 UTM as per ASTM D790 standard at a crosshead speed of 0.77 mm/min. The dimension of sample specimen is 3.2 × 12.7 × 165 mm. The flexural strength (FS) of the specimen is calculated as follows:

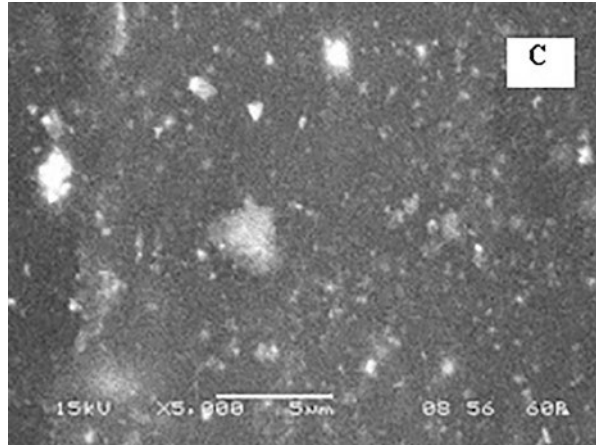**Fig. 2** SEM image of HAp-HDPE composite at 30 vol. % of HAp



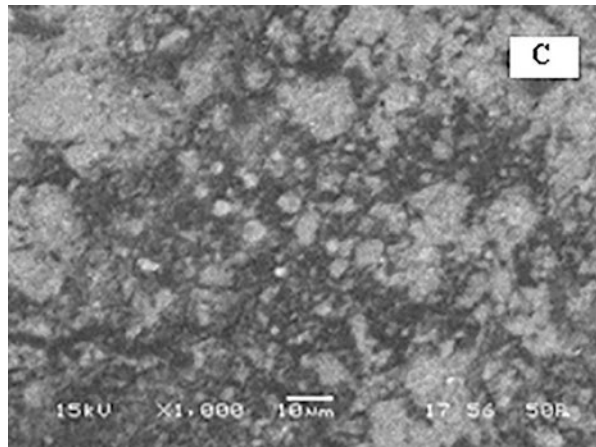**Fig. 3** SEM image of HAp-UHMWPE at 30 vol. % of HAp



**Table 1** Specifications of all the testing machines

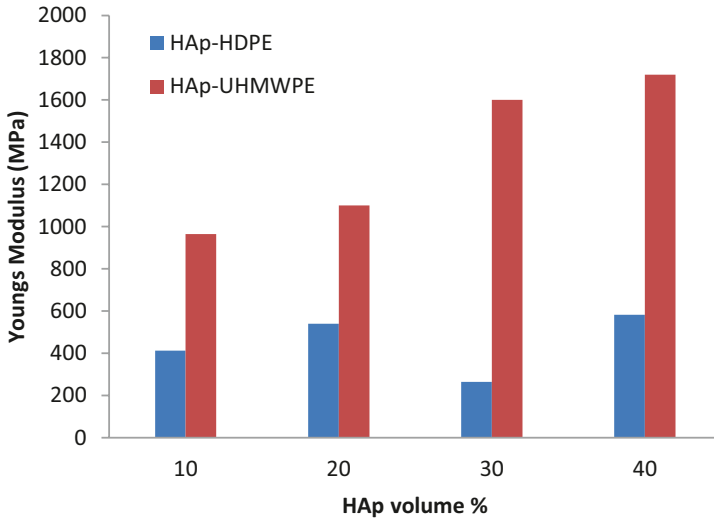|  | Machine used | Variables | Standard used |
|---|---|---|---|
| Tensile | INSTRON 3382 UTM | Load cell: 100 KN Rate: 10 mm/min | ASTM D638 |
| Compressive | INSTRON 3382 UTM | Rate: 1.3 mm/min | ASTM D695 |
| Flexural | INSTRON 3382 UTM | Rate: 0.77 mm/min | ASTM D790 |
| Impact | Tinius Olsen Impact Systems IT406 | – | ASTM D256 |

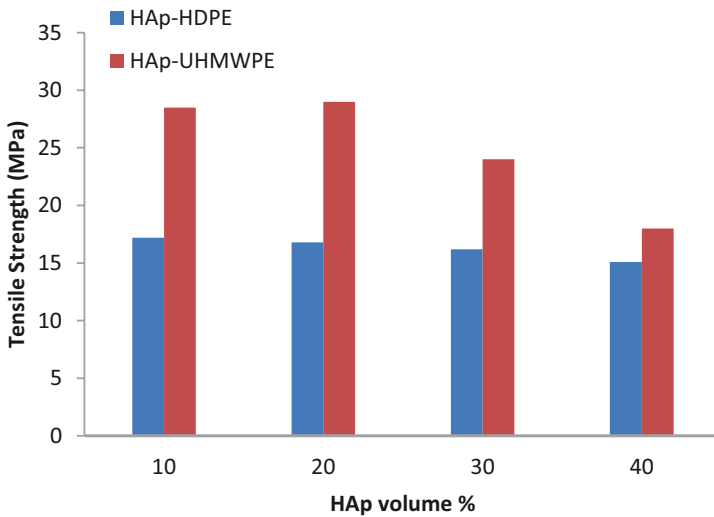**Fig. 4** Plot of Young's modulus versus HAp vol. %



**Fig. 5** Effects of HAp contents on the tensile strength

$$FS = \frac{3P.L}{b.t^3}$$

$$(1)$$

where $P$ is the maximum load, $b$ is the width, $t$ is the thickness, and $L$ is the length
of the specimen. The data recorded in the flexural test is also used to determine the
inter-laminar shear stress (ILSS)) values calculated as follows:
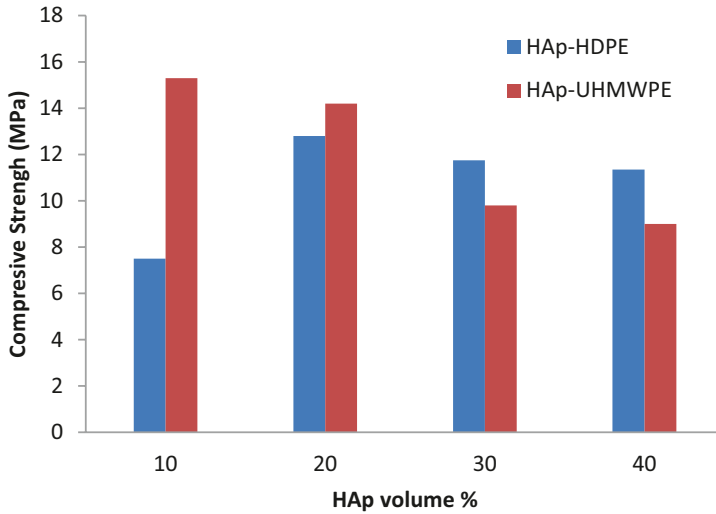
**Fig. 6** Effects of HAp contents on the compressive strength



**Fig. 7** Effects of HAp contents on the flexural strength

$$\text{LSS} = \frac{3P}{4b.t}$$

(2)

The flexural properties are of great importance for any structural element. Biocompatible composite used in hip joints may fail in bending loads, and therefore, the development of new composites with improved flexural characteristics is desirable. Figure 7 shows that flexural strength of HAp-UHMWPE composite is

**Fig. 8** Reinforcement effect of HAp on ILSS)
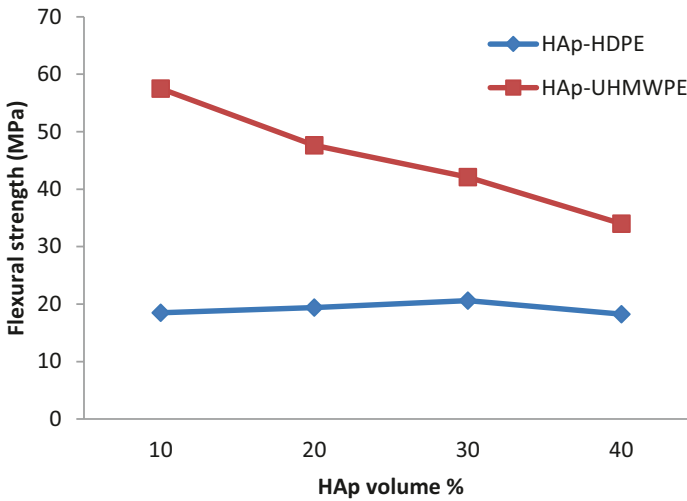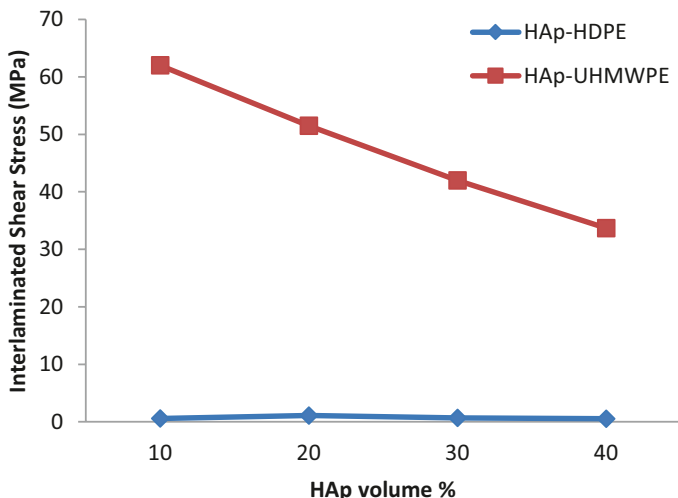
higher than HAp-HDPE composite for any value of HAp content. However, flexural strength decreases with increase of HAp volume % for HAp-UHMWPE composite. No appreciable change in flexural strength is noticed for HAp-HDPE composite with increase in HAp content. Figure 8 shows the plot between HAp vol. % versus ILSS) in which 20 vol. % of HAp gives maximum ILSS) for HAp-HDPE, but the plot between HAp vol. % versus ILSS for HAp-UHMWPE composite shows decrease of ILLS with increase in HAp content.

The tensile properties of HAp-HDPE and HAp-HMHDPE composites at 20% vol. of HAp are compared with previous studies. The present study gives a tensile strength of 17.18 MPa, whereas past studies report tensile strength as 17.65–19.97 MPa [35–37] for HAp-HDPE composites. The strength values reported in the present study is comparable with past studies. It is observed that the present study gives a tensile strength of 28.21 MPa, whereas Fang et al. [38] obtained the tensile strength of 26.67 MPa.

## 2.2 Drilling of Composites

Drilling is a cutting process that uses a drill bit to cut or enlarge a hole of circular cross-section in solid materials. The composites under study being softer than most metals, drilling of composite is considerably easier and faster. Cutting fluids are not used or needed. Here, the effect of different parameter settings on circularity at entry and exit and hole taper on HAp-HDPE composite is analyzed. The thickness

**Table 2**  Drilling parameters and with levels

| Machining parameters | Level 1 | Level 2 | Level 3 | Level 4 |
|---|---|---|---|---|
| HAp (vol. %) | 10 | 20 | 30 | 40 |
| Feed rate (mm/min) | 50 | 100 | 150 | 200 |
| Speed (rpm) | 750 | 1500 | 2250 | 3000 |
| Drill diameter (mm) | 5 | 6 | | |

**Table 3**  Taguchi's mixed-level $L_{16}$ orthogonal array combinations

| Experimental runs | HAp (vol. %) | Feed rate (mm/min) | Speed (rpm) | Drill diameter (mm) |
|---|---|---|---|---|
| 1 | 10 | 50 | 750 | 5 |
| 2 | 10 | 100 | 1500 | 5 |
| 3 | 10 | 150 | 2250 | 6 |
| 4 | 10 | 200 | 3000 | 6 |
| 5 | 20 | 50 | 1500 | 6 |
| 6 | 20 | 100 | 750 | 6 |
| 7 | 20 | 150 | 3000 | 5 |
| 8 | 20 | 200 | 2250 | 5 |
| 9 | 30 | 50 | 2250 | 5 |
| 10 | 30 | 100 | 3000 | 5 |
| 11 | 30 | 150 | 750 | 6 |
| 12 | 30 | 200 | 1500 | 6 |
| 13 | 40 | 50 | 3000 | 6 |
| 14 | 40 | 100 | 2250 | 6 |
| 15 | 40 | 150 | 1500 | 5 |
| 16 | 40 | 200 | 750 | 5 |

of the composite sample is measured at different sections with a digital vernier caliper with least count of 0.01 mm. Then, drilling process are done on the composite work piece at different parameter settings. The diameters of the drilled holes are in millimeter range, and the holes are drilled without any relative motion between the job and the workpiece. The experiments were done on a CNC MAXMILL machine system. The drilling operation is done on HAp-HDPE composite work piece with a mean thickness of 3.03 mm, 2.95 mm, 3.12 mm, and 3.18 mm for 10 vol. %, 20 vol. %, 30 vol. %, and 40 vol. %, respectively. The controllable parameters considered with their levels are shown in Table 2. Experiments are carried out using Taguchi's $L_{16}$ orthogonal array. The factorial combinations for experimental runs are shown in Table 3. The drilling operation is shown in Fig. 9.

**Fig. 9** Drilling operation



## 3 Multi-response Optimization Using Principal Component Analysis

Principal component analysis is a projection-based technique that facilitates reduction in data dimension through the construction of orthogonal principal components that are weighted linear combinations of the original variables. To optimize the multiple responses into a single equivalent response, various methods are used. However, the responses may be correlated among themselves. Therefore, the responses must be uncorrelated before finding an equivalent response. Tong et al. [22] have used principal component analysis along with technique for order preference by similarity to ideal solution (TOPSIS) for multiple response optimization of processing thin films to be used in integrated circuit [22]. Liu et al. introduces PCA algorithm for network wide traffic anomaly detection in a distributed fashion [39]. Here, the effect of important drilling parameters like HAp vol. %, feed, speed, and drill diameter on the responses such as taper, circularity at entry, and circularity at exit are considered. The multi-responses are converted into a single response using principal component analysis (PCA); hence, the influence of correlation among the responses can be eliminated. Steps including for the procedure are as follows:

Step 1. Normalize the responses [21] by using the Eqs. (3) and (4) for larger the better and smaller the criterion, respectively. Since taper is to be minimized, smaller-the-better criterion is to be used. As the circularity at entry and exit is expressed as the ratio of minimum Farret diameter to maximum Farret diameter, it is maximized using larger-the-better characteristic is used.

$$\text{Larger the better}, Y_{ij} = \frac{L_{ij} - \min\left(L_j\right)}{\max\left(L_j\right) - \min\left(L_j\right)}$$

(3)

$$\text{Smaller the better,} Y_{ij} = \frac{\max\left(L_j\right) - L_{ij}}{\max\left(L_j\right) - \min\left(L_j\right)}$$

(4)

Step 2. Calculate the PCA on the normalized values of the responses to obtain principal component scores (PCSs) [36], to find the eigen values and vectors for the corresponding responses by getting the relation PCS$_{ij}$, computing $(g)_{m \times p}$ to PCA, the value of $i$th $(i = 1, 2,…, p)$ PCS corresponding to $i$th trial, (PCS$_{il}$) can be obtained as follows:

$$\text{PCS}_{il} = a_{k1}n_{i1} + a_{k2}n_{i2} + … + a_{kp}n_{ip}$$

(5)

where $a_{k1}, a_{k2},…,a_{kp}$ are the eigen vectors with respect to eigenvalues ($k$th terms) of the matrix.

Step 3. Next we have to perform normalization of the PCSs ($X_{il}$) values [39], by the following equation:

$$X_{il} = \frac{\text{PCS}_{il} - \min\left(\text{PCS}_1\right)}{\max\left(\text{PCS}_1\right) - \min\left(\text{PCS}_1\right)}$$

(6)

Step 4. Three principal components are obtained using PCA, that principal component 1 (PC1) has $V_1$ of variance, (PC2) has $V_2$, and (PC3) has $V_3$ of total variance. The relation for weighted principal component, WPC, is given by equation:

$$\text{WPC} = \left(V_1 \times \text{PCS1}\right) + \left(V_2 \times \text{PCS3}\right) + \left(V_3 \times \text{PCS3}\right)$$

(7)

## 4 Results and Discussions

The effect of different drilling parameters on circularity at entry and exit and hole taper on HAp-HDPE bio-composite is analyzed. The circularity at both entry and exit is calculated by using the ratio of minimum to maximum diameters of the hole. After measuring the entrance diameter and exit diameter of the hole, the hole taper is calculated by Eq. (8).

$$\text{Hole taper } \left(\text{in radian}\right) = \frac{\left(\text{hole enterance diameter}\right) - \left(\text{hole exit diameter}\right)}{\left(2 \times \text{thickness of the workpiece}\right)}$$

(8)

The output responses are calculated for taper, circularity at entry, and circularity at exit as shown in Table 4.

**Table 4** Design of $L_{16}$ experiments and its observations

| Sl. No. | HAp (vol. %) | Feed rate (mm/min) | Speed (rpm) | Drill diameter (mm) | Taper (radian) | Circularity at entry (mm) | Circularity at exit (mm) |
|---|---|---|---|---|---|---|---|
| 1 | 10 | 50 | 750 | 5 | 0.0242 | 0.9642 | 0.8217 |
| 2 | 10 | 100 | 1500 | 5 | 0.0098 | 0.8415 | 0.7821 |
| 3 | 10 | 150 | 2250 | 6 | 0.0018 | 0.8495 | 0.8388 |
| 4 | 10 | 200 | 3000 | 6 | 0.0020 | 0.8666 | 0.8544 |
| 5 | 20 | 50 | 1500 | 6 | 0.0046 | 0.8356 | 0.8084 |
| 6 | 20 | 100 | 750 | 6 | 0.0017 | 0.845 | 0.835 |
| 7 | 20 | 150 | 3000 | 5 | 0.0006 | 0.8352 | 0.8314 |
| 8 | 20 | 200 | 2250 | 5 | 0.0009 | 0.8554 | 0.8502 |
| 9 | 30 | 50 | 2250 | 5 | 0.0056 | 0.8514 | 0.8166 |
| 10 | 30 | 100 | 3000 | 5 | 0.0040 | 0.8379 | 0.8128 |
| 11 | 30 | 150 | 750 | 6 | 0.0003 | 0.8402 | 0.8383 |
| 12 | 30 | 200 | 1500 | 6 | 0.0009 | 0.8374 | 0.8316 |
| 13 | 40 | 50 | 3000 | 6 | 0.0037 | 0.8238 | 0.8000 |
| 14 | 40 | 100 | 2250 | 6 | 0.0023 | 0.8272 | 0.8125 |
| 15 | 40 | 150 | 1500 | 5 | 0.0008 | 0.8238 | 0.8187 |
| 16 | 40 | 200 | 750 | 5 | 0.0019 | 0.8474 | 0.8352 |

**Table 5** Eigenvalues, eigenvectors, accountability proportion (AP), and cumulative variation (CV) computed for the first three major quality indicators

| Principal component | Eigen value | Explained variation | Cumulative variation (%) | Eigen vector (taper, circularity at entry, circularity at exit) |
|---|---|---|---|---|
| PC1 | 1.8701 | 0.623 | 0.623 | [0.723, −0.671, 0.163] |
| PC2 | 1.1298 | 0.377 | 1 | [−0.140, −0.374, −0.917] |
| PC3 | 0.0001 | 0.000 | 1 | [−0.676, −0.640, 0.364] |

## 4.1 Principal Component Analysis

Optimization of the observed data has been done in Table 4, by using the responses and normalized by the Eqs. (1) and (2) and formulated in Minitab 16 which gives the eigen values and vectors tabulated in Table 5.

The PCS values were obtained using Eq. (3) and normalized by using Eq. (4). This is further optimized by using Eq. (5) tabulated in Table 4 to get the weighted WPC. Tables 6 and 7 shows the optimum condition obtained using Minitab 16. An $L_{16}$ array is performed to get the analysis of variance (ANOVA) and signal-to-noise ratio shown in Tables 8 and 9, for the study of machining parameters showing the s/n ratio plot of WPC in Fig. 10.

The main effects plot for means of SN ratios of WPC as in Fig. 10. Here, higher-the-better (HTB) value is considered, and it shows the optimum parametric setting as $A_1B_1C_2D_1$. That is, feed rate of 50 mm/min, speed of 1500 rpm, and 5 mm drill diameter for drill in 10 vol. % of HAp sample, and then we get minimum taper with maximum circularity at both entry and exit [40–45].

**Table 6** Principal component analysis for $L_{16}$ experimental observations

| Sl. No. | Normalization of outputs $Y_{ij}$ | | | Principal components | | |
|---|---|---|---|---|---|---|
| | $Y_{1j}$ | $Y_{2j}$ | $Y_{3j}$ | PCS1 | PCS2 | PCS3 |
| 1 | $6.56 \times 10^{-6}$ | 0 | −0.45228 | −0.0737 | 0.414742 | −0.16464 |
| 2 | 0.60583 | −0.87393 | −1 | 0.86144 | 1.15903 | −0.21424 |
| 3 | 0.96091 | −0.81695 | −0.21577 | 1.20774 | 0.368871 | −0.20527 |
| 4 | 0.94997 | −0.69516 | 0 | 1.15328 | 0.126992 | −0.19728 |
| 5 | 0.83524 | −0.91595 | −0.63624 | 1.11477 | 0.809063 | −0.21000 |
| 6 | 0.96404 | −0.849 | −0.26833 | 1.22294 | 0.428617 | −0.20600 |
| 7 | 1.01047 | −0.9188 | −0.31812 | 1.29523 | 0.493882 | −0.21084 |
| 8 | 0.99998 | −0.77493 | −0.05809 | 1.23349 | 0.203095 | −0.20118 |
| 9 | 0.79253 | −0.80342 | −0.52282 | 1.02687 | 0.668952 | −0.21187 |
| 10 | 0.86120 | −0.89957 | −0.57538 | 1.13248 | 0.743495 | −0.21589 |
| 11 | 1.02547 | −0.88319 | −0.22268 | 1.29774 | 0.390948 | −0.20903 |
| 12 | 0.99786 | −0.90313 | −0.31535 | 1.27605 | 0.48725 | −0.21133 |
| 13 | 0.87359 | −1 | −0.75242 | 1.17996 | 0.941667 | −0.22443 |
| 14 | 0.93681 | −0.97578 | −0.57953 | 1.23759 | 0.765219 | −0.21973 |
| 15 | 1.00349 | −1 | −0.49378 | 1.31604 | 0.686303 | −0.2181 |
| 16 | 0.95417 | −0.83191 | −0.26556 | 1.20479 | 0.421068 | −0.20926 |

**Table 7** Weighted principal component for $L_{16}$ experimental observations

| Sl. No. | Normalized principal components $X_{il}$ | | | WPC | S/N ratio of WPC |
|---|---|---|---|---|---|
| | $PCS_{1l}$ | $PCS_{2l}$ | $PCS_{3l}$ | | |
| 1 | 0.999 | 0.278 | 1.000 | 0.728 | −2.756 |
| 2 | 0.327 | 1 | 0.170 | 0.581 | −4.719 |
| 3 | 0.078 | 0.234 | 0.321 | 0.137 | −17.27 |
| 4 | 0.117 | $-2.9 \times 10^{-7}$ | 0.454 | 0.073 | −22.74 |
| 5 | 0.145 | 0.661 | 0.241 | 0.339 | −9.386 |
| 6 | 0.067 | 0.293 | 0.308 | 0.152 | −16.36 |
| 7 | 0.015 | 0.355 | 0.227 | 0.143 | −16.87 |
| 8 | 0.059 | 0.074 | 0.389 | 0.065 | −23.77 |
| 9 | 0.208 | 0.525 | 0.210 | 0.328 | −9.693 |
| 10 | 0.132 | 0.597 | 0.143 | 0.307 | −10.24 |
| 11 | 0.013 | 0.256 | 0.258 | 0.105 | −19.61 |
| 12 | 0.029 | 0.349 | 0.219 | 0.149 | −16.51 |
| 13 | 0.098 | 0.789 | $2.3 \times 10^{-5}$ | 0.359 | −8.908 |
| 14 | 0.056 | 0.618 | 0.079 | 0.268 | −11.43 |
| 15 | $2.5 \times 10^{-7}$ | 0.542 | 0.106 | 0.204 | −13.79 |
| 16 | 0.080 | 0.285 | 0.254 | 0.157 | −16.07 |

**Table 8** ANOVA for SN ratios

| Source | DF | Seq SS | Adj SS | Adj MS | F | P |
|---|---|---|---|---|---|---|
| HAp volume (%) | 3 | 52.62 | 52.62 | 17.54 | 2.6 | 0.164 |
| Feed rate (mm/min) | 3 | 368.84 | 368.84 | 122.946 | 18.25 | 0.004 |
| Speed (rpm) | 3 | 44.42 | 44.42 | 14.808 | 2.2 | 0.207 |
| Drill diameter (mm) | 1 | 36.91 | 36.91 | 36.907 | 5.48 | 0.066 |
| Residual error | 5 | 33.68 | 33.68 | 6.736 | – | – |
| Total | 15 | 536.47 | – | – | – | – |

**Table 9** Response table for SN ratios

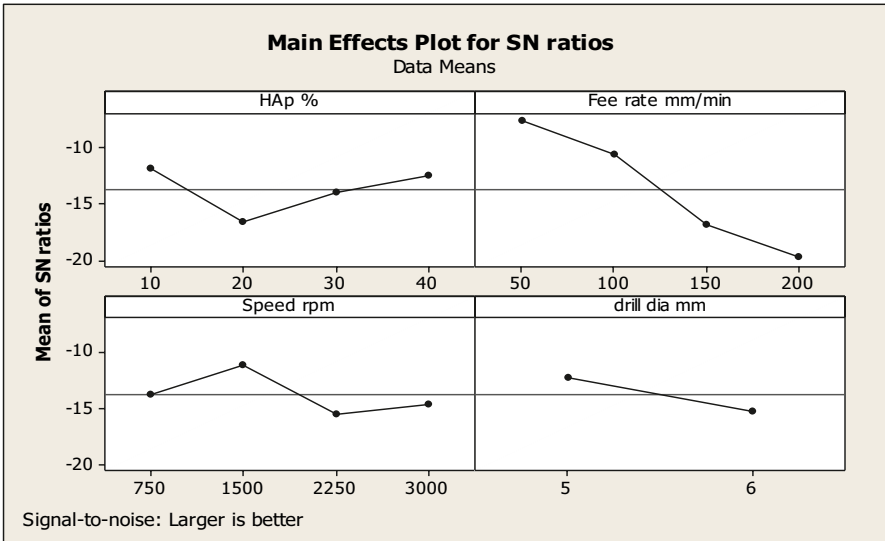| Level | HAp (vol. %) | Feed rate (mm/min) | Speed (rpm) | Drill diameter (mm) |
|---|---|---|---|---|
| 1 | −11.871 | −7.686 | −13.699 | −12.239 |
| 2 | −16.599 | −10.69 | −11.101 | −15.276 |
| 3 | −14.012 | −16.886 | −15.54 | – |
| 4 | −12.549 | −19.769 | −14.69 | – |
| Delta | 4.727 | 12.084 | 4.439 | 3.038 |
| Rank | 2 | 1 | 3 | 4 |



**Fig. 10** Main effects plot for means of SN ratios

## 4.2 Estimation of Optimum Performance of Parameters

The optimum drilling parameters were analyzed by taking SN ratios of WPC, parameters are $A_4$, $B_1$, $C_2$, and $D_1$. Therefore, the predicted mean of parameters has been calculated [46] by Eq. (9)

$$S_{s/n} = \bar{Y} + \left(\bar{A}_1 - \bar{Y}\right) + \left(\bar{B}_1 - \bar{Y}\right) + \left(\bar{C}_2 - \bar{Y}\right) + \left(\bar{D}_1 - \bar{Y}\right) \tag{9}$$

where $\bar{Y}$ is the total average of s/n ratios (of MPI from Table 5), $\bar{A}_1$, $\bar{B}_1$, $\bar{C}_2$, and $\bar{D}_1$ are the s/n ratios of the average drilling parameters at the optimal levels, and $S_{s/n}$ denotes the predicted signal to noise ratio. Therefore, the calculated values of the responses are $\bar{Y} = -13.7576$, $\bar{A}_1 = -11.8713$, $\bar{B}_1 = -7.6857$, $\bar{C}_2 = -10.6873$, and $\bar{D}_1 = -12.2385$ (from Table 5). Substituting the values in Eq. (7), the predicted mean parameter is: $S_{s/n} = -1.2099$.

The confidence interval for the predicted [47] mean of SN ratio is given by Eqs. (10) and (11).

$$CI = \sqrt{F_\alpha\left(1; f_e\right).V_e\left[\frac{1}{N_{\text{eff}}} + \frac{1}{R}\right]} \tag{10}$$

$$N_{\text{eff}} = \frac{N}{1 + T_{\text{DOF}}} \tag{11}$$

where, $F_\alpha(1; f_e)$ is the F ratio required for $100(1 - \alpha)$ percent confidence interval, $f_e$ is error degree of freedom, $V_e$ error variance is 6.736 (from Table 7), $R$ is the number of replication, $N$ the number of experiment, and $T_{\text{DOF}}$ the total degrees of freedom (from Table 6).

Substituting the values in Eq. (10), the calculated confidence interval is: $CI = \pm 8.66809$. The 95% confidence interval of the predicted optimal parameters is obtained as:

$$7.4582 < S_{s/n} < -9.8780$$

## 4.3 Confirmation Experiment

The confirmation experiment was performed on the parameters 10% HAp, 50 mm/min feed rate, 1500 rpm speed, and 6 mm drill diameter (i.e., $A_1B_1C_2D_2$), thus confirmation s/n ratio of WPC is $-4.99678$, thus which is under predicted optimal parameters.

# 5 Conclusions

This chapter presents a methodology using principal component analysis embedded with Taguchi method for simultaneous optimization of multiple responses of correlated in nature. The application of includes drilling of bio-composites (HAp and HDPE) extensively used in bone grafting. The optimum combination of drilling parameters can lead to minimum taper with maximum circularity at entry and exit. The optimal parameters are listed as feed rate of 50 mm/min, speed of 1500 rpm, and drill diameter of 5 mm for drilling of composites containing HAp of 10% (vol. %). Optimization of performance measures suggest PCA is a robust technique. The confirmation test shows the adequacy of the proposed methodology.

# References

1. Venkatesan, J., & Kim, S. K. (2010). Effect of temperature on isolation and characterization of hydroxyapatite from tuna (Thunnusobesus) bone. *Materials, 3*, 4761–4772.
2. Fratzl, P., Gupta, H., Paschalis, E., & Roschger, P. (2004). Structure and mechanical quality of the collagen–mineral nano-composite in bone. *Journal of Materials Chemistry, 14*, 2115–2123.
3. Chowdhury, Kulkarni, A. C., Basak, A., & Roy, S. K. (2007). Wear characteristic and biocompatibility of some hydroxyapatite-collagen composite acetabular cups. *Wear, 262*(11-12), 1387–1398.
4. Tang, P., Li, G., Wang, J., Zheng, Q., & Wang, Y. (2009). Development, characterization, and validation of porous carbonated hydroxyapatite bone cement. *Journal of Biomedical Materials Research Part B, 90*, 886–893.
5. Kothamasu, R., & Haung, S. H. (2007). Adaptive Mamdani fuzzy model for condition-based maintenance. *Fuzzy Sets and Systems, 158*, 2715–2733.
6. Kmita, R. A., Slosarczyk, A., & Paszkiewicz, Z. (2006). Mechanical properties of HAp–ZrO$_2$ composites. *Journal of the European Ceramic Society, 26*(8), 1481–1488.
7. Park, M. S., Eanes, E. D., Antonucci, J. M., & Skrtic, D. (1998). Mechanical properties of bioactive amorphous calcium phosphate/methacrylate composites. *Dental Materials, 14*(2), 137–141.
8. Veljovic, D., Zalite, I., Palcevskis, E., Smiciklas, I., Petrovic, R., & Janakovic, D. (2010). Microwave sintering of fine-grained HAP and HAP/TCP bioceramics. *Ceramics International, 36*(2), 595–603.
9. Jaggi, H. S., Kumar, Y., Satapathy, B. K., Ray, A. R., & Patnaik, A. (2012). Analytical interpretations of structural and mechanical response of high density polyethylene/hydroxyapatite bio-composites. *Materials & Design, 36*, 757–766.
10. Ge, S., Wang, S., & Haung, X. (2009). Increasing the wear resistance of UHMWPE acetabular cups by adding natural biocompatible particles. *Wear, 267*(5–8), 770–776.
11. Deie, M., Ochi, M., Adachi, N., Nishimori, M., & Yokota, K. (2008). Artificial bone grafting [calcium hydroxyapatite ceramic with an interconnected porous structure (IP-CHA)] and core decompression for spontaneous osteonecrosis of the femoral condyle in the knee. *Knee Surgery, Sports Traumatology, Arthroscopy, 16*, 753–758.
12. Noriyukitamai, A., Ikuokudawara, T., & Hidekiyoshikawa, N. (2010). Fully interconnected porous hydroxyapatite ceramic in surgical treatment of benign bone tumor. *Journal of Orthopaedic Science, 15*, 560–568.

13. Yoshikawa, H., & Myoui, A. (2005). Bone tissue engineering with porous hydroxyapatite ceramics. *The Japanese Society for Artificial Organs, 8*, 131–136.
14. Kuriyama, K., Hashimoto, J., Murase, T., Fujii, M., Nampei, A., Hirao, M., Tsuboi, H., Myoui, A., & Yoshikawa, H. (2009). Treatment of juxta-articular intraosseous cystic lesions in rheumatoid arthritis patients with interconnected porous calcium hydroxyapatite ceramic. *Official Journal of Japan College of Rheumatology, 19*, 180–186.
15. Yoshida, Y., Osaka, S., & Tokuhashi, Y. (2009). Clinical experience of novel interconnected porous hydroxyapatite ceramics for the revision of tumor prosthesis: a case report. *World Journal of Surgical Oncology, 7*, 76.
16. Choubey, A., Chaturvedi, V., & Vimal, J. (2012). The implementation of Taguchi methodology for optimization of end milling process parameter of mild steel. *International Journal of Engineering, Science and Technology, 4*(7), 3261–3267.
17. Ross, P. J. (1995). *Taguchi techniques for quality engineering*. McGraw Hill.
18. Pahadke, M. S. (1989). *Quality engineering using robust design*. Prentice-Hall.
19. Tsao, C. C., & Hocheng, H. (2007). Parametric study on thrust force of core drill. *Journal of Materials Processing Technology, 192–193*, 37–40.
20. Kilickap, E. (2010). Modeling and optimization of burr height in drilling of Al-7075 using Taguchi method and response surface methodology. *The International Journal of Advanced Manufacturing Technology, 49*, 911–923.
21. Huang, M. S., & Lin, T. Y. (2008). Simulation of a regression-model and PCA based searching method developed for setting the robust injection molding parameters of multi-quality characteristics. *International Journal of Heat and Mass Transfer, 51*, 5828–5837.
22. Tong, L. I., Wang, C. H., & Chen, H. C. (2005). Optimization of multiple responses using principal component analysis and technique for order preference by similarity to ideal solution. *The International Journal of Advanced Manufacturing Technology, 27*, 407–414.
23. Liu, Y., Zhang, L., & Guan, Y. (2010). Sketch-based streaming PCA algorithm for network-wide traffic anomaly detection. *International Conference on Distributed Computing Systems, 1*, 807–808.
24. Salmasnia, A., Kazemzadeh, R. B., Esfahani, M. S., & Hejazi, T. H. (2013). Multiple response surface optimization with correlated data. *The International Journal of Advanced Manufacturing Technology, 64*, 841–855.
25. Sun, Y., Zeng, W., Zhao, Y., Shao, Y., & Zhou, Y. (2012). Modeling the correlation of composition-processing-property for TC11 titanium alloy based on principal component analysis and artificial neural network. *Journal of Materials Engineering and Performance, 21*, 2231–2237.
26. Bin, C. Y., & Shui, L. C. (2008). Blended coal's property prediction model based on PCA and SVM. *Journal of Central South University of Technology, 15*(2), 331–335.
27. Qiang, Z., Jun, M., & Fei, D. (2008). Optimization design of drilling string by screw coal miner based on ant colony algorithm. *Journal of Coal Science and Engineering (China), 14*(4), 686–688.
28. Barbosa, M. C., Messmer, N. R., Brazil, M., & Lobo, A. O. (2013). The effect of ultrasonic irradiation on the crystallinity of nano-hydroxyapatite produced via the wet chemical method. *Materials Science and Engineering C, 1*, 1–6.
29. Yuana, Q., Yang, Y., Chen, J., Ramuni, V., Misra, R. D. K., & Bertrand, K. J. (2010). The effect of crystallization pressure on macromolecular structure, phase evolution, and fracture resistance of nano-calcium carbonate-reinforced high-density polyethylene. *Materials Science and Engineering A, 527*, 6699–6713.
30. Wang, P., Li, C., Gong, H., Jiang, X., Wang, H., & Li, K. (2010). Effects of synthesis conditions on the morphology of hydroxyapatite nanoparticles produced by wet chemical process. *Powder Technology, 203*, 315–321.
31. Bing, A., Hi, C. X., Shun, W. F., & Ping, W. Y. (2010). Preparation of micro-sized and uniform spherical Ag powders by novel wet-chemical method. *Transactions of Nonferrous Metals Society of China, 20*, 1550–1554.

32. Saeri, M. R., Afshar, A., Ghorbani, M., Ehsani, N., & Sorrell, C. C. (2003). The wet precipitation process of hydroxyapatite. *Materials Letters, 57*, 4064–4069.
33. Velayudhan, S., Ramesh, P., Sunny, M. C., & Varma, H. K. (2000). Extrusion of hydroxyapatite to clinically significant shapes. *Materials Letters, 46*(2), 142–146.
34. Abu, B. M. S., Cheang, P., & Khor, K. A. (2003). Mechanical properties of injection molded HAp-PEEK bio-composites. *Composites Science and Technology, 63*(3-4), 421–425.
35. Wang, M., Joseph, R., & Bonfield, W. (1998). Hydroxyapatite-polyethylene composites for bone substitution: Effects of ceramic particle size and morphology. *Biomaterials, 19*(24), 2357–2366.
36. Wang, M., & Bonfield, W. (2001). Chemically coupled hydroxyapatite-polyethylene composites: Structure and properties. *Biomaterials, 22*, 1311–1320.
37. Ryan, K. R., Sproul, M. M., & Turner, C. H. (2003). Hydroxyapatite whiskers provide improved mechanical properties in reinforced polymer composites. *Journal of Biomedical Materials Research Part A, 67*, 801–812.
38. Fang, L., Leng, Y., & Gao, P. (2006). Processing and mechanical properties of HA/UHMWPE Nano composites. *Biomaterials, 27*, 3701–3707.
39. Liu, Y., Zhang, L., & Guan, Y. (2010). Sketch-based streaming PCA algorithm for network-wide traffic anomaly Detection. *International Conference on Distributed Computing System, 2010*, 807–816.
40. Ali Salmasnia, A., & Kazemzadeh, R. B. (2013). Multiple response surface optimization with correlated data. *The International Journal of Advanced Manufacturing Technology, 64*, 841–855.
41. Chakravorty, R., Gauri, S. K., & Chakraborty, S. (2012). Optimization of correlated responses of EDM process. *Materials and Manufacturing Processes, 27*, 337–347.
42. Kilickap, E. (2010). Determination of optimum parameters on delamination in drilling of GFRP composites by Taguchi method. *Indian Journal of Engineering & Materials Sciences, 17*(4), 265–274.
43. Biswas, R., Kuar, A. S., Sarkar, S., & Mitra, S. (2010). A parametric study of pulsed Nd:YAG laser micro-drilling of gamma-titanium aluminide. *Journal of Optics and Laser Technology, 42*(1), 23–31.
44. Ajaal, T. T., & Smith, R. W. (2008). Employing the Taguchi method in optimizing the scaffold production process for artificial bone graft. *Journal of Materials Processing Technology, 209*(4), 1521–1532.
45. Gopalsamy, B. M., Mondal, B., & Ghosh, S. (2009). Taguchi method and ANOVA: An approach for process parameters optimization of hard machining while machining hardened steel. *Journal of Scientific and Industrial Research, 68*(8), 686–695.
46. Chaulia, P. K., & Das, R. (2008). Process parameter optimization for fly ash brick by Taguchi method. *Materials Research, 11*(2), 159–164.
47. Singh, H., & Kumar, P. (2004). Tool wear optimization in turning operation by Taguchi method. *Indian Journal of Engineering & Materials Sciences, 11*(1), 19–24.